# Inelastic Neutron Scattering on Si from 4 to 20 MeV at FIGARO

D. Rochman, R. C. Haight, J. M. O'Donnell and M. Devlin
*LANSCE-3, Los Alamos National Laboratory, NM 87545, USA*
*rochman@lanl.gov, haight@lanl.gov, odonnell@lanl.gov, devlin@lanl.gov*

**Abstract**-*The energy spectrum of the outgoing neutrons from the reaction Si(n,n'γ)Si is studied as a function of incident neutron energy, using the white neutron beam of the WNR facility at the Los Alamos Neutron Science Center (LANSCE) and the FIGARO facility. To signal an inelastic scattering event, γ-rays of $E_\gamma$ = 1.78 MeV, characteristic of the transition in $^{28}$Si between the first-excited and ground states, are detected by one high-resolution Ge or one barium-fluoride detector. The emitted neutrons are detected by six liquid scintillators (EJ301) at about 1 meter from the sample so that the time of flight of the emitted neutron can be measured and its energy deduced. The excitation function of the emission spectrum for incident neutron energies $E_n$ = 4 to 20 MeV is then obtained and compared with the predictions of the nuclear model calculations performed with the codes GNASH and EMPIRE II. Furthermore, a comparison is made with the calculations and with experimental data from the literature.*

## I. INTRODUCTION

Understanding nuclear reactions and nuclear structure is key to reliable calculations regarding nuclear weapons, transmutation of radioactive waste from power reactors, neutron transport, radiation effects and synthesis of the elements in stars. Nucleon inelastic scattering is potentially a very powerful probe of nuclear structure and gives access to the transition probabilities between the nuclear ground state and the excited states. In this goal, the new Fast Neutron-Induced Gamma-Ray Observer (FIGARO) was constructed on a flight path at the Weapons Research Facility (WNR)[1] to measure γ-ray and neutron emission spectra following neutron-induced reactions.

In natural silicon, $^{28}$Si has an abundance of 92.2 % and thus is a simple target for a first experimental study and for testing model calculations. Silicon is also of great applied interest in the semiconductor industry and in detectors for physics experiments. Neutron-induced reactions have been known for many years to be responsible for producing errors in semiconductor memories.[2] Several measurements have been performed on Si samples for neutron inelastic scattering[3−8] with mono-energetic neutrons at several incident neutron energies but not over the complete range from threshold to 20 MeV. Three studies on $^{28}$Si present some results about the excitation function: Ref. 9 presents the spectra of neutrons scattered inelastically to the first excited state with the excitation function at 60° for an incident neutron energy from 2 to 6 MeV, Ref. 10 presents an excitation function to the $2^+$ state of the integrated inelastic cross section for several incident neutron energies from 6.8 to 14.8 MeV and Ref. 11 presents the excitation function of the emission spectrum for an incident neutron energy of 14.1 MeV.

In general neutron-induced reactions, the residual nucleus is in a highly excited state which subsequently decays via a γ cascade to the ground state or via neutron or light-charged particle emission. Direct transitions to the ground state are unlikely because of the many other decay modes possible. For even-even nuclei, because there is sufficient angular momentum in the system to populate a rather wide range of residual states, few of these states, except the lowest $2^+$ state, decay directly to the ground state and nearly all decay through this $2^+$ state, see Fig 1.

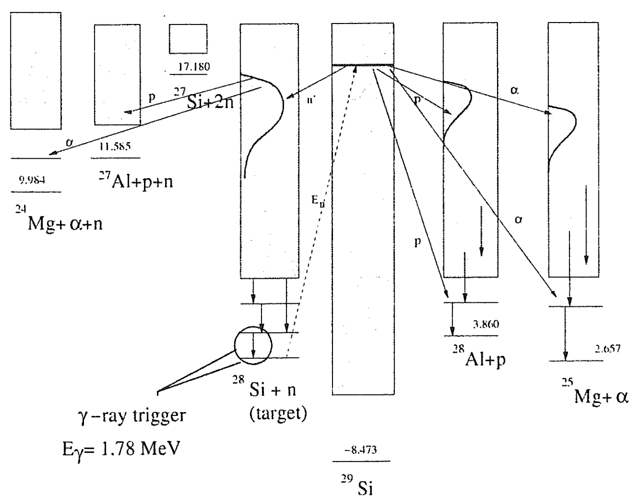


FIG. 1: $(n,n')$, $(n,n'p)$, $(n,n'\alpha)$, $(n,p)$ and $(n,\alpha)$ channels for the reaction $^{28}$Si+$n$.

Thus, for incident neutron energies lower than the effective threshold for the $(n,2n)$ [$Q = -17.18$ MeV], $(n,n'p)$ [$Q = -11.58$ MeV] or $(n,n'\alpha)$ [$Q = -9.98$ MeV] reactions, the measurement of the cross section of $^{28}$Si$(n,n')^{28}$Si in coincidence with the 1.78 MeV transition from the $2^+$ excited state to the ground state is approximately equal to the measurement of the inelastic cross section.

FIGARO is a flexible facility at WNR for the study of neutron-induced reactions that result in the emission of γ-rays and neutrons. It is designed for high-resolution γ-ray detection from neutron-induced interactions with selected target nuclei, with the possibility of detecting neutrons emitted in the reaction over a continuous wide range of incident neutron energies from 1 MeV to more than 100 MeV.



## II. EXPERIMENTAL PROCEDURE

### I.A. Set-up

The experiments were performed at the 30° right flight path of the WNR facility. The general features of the 30° right flight path setup are described in Ref. 12. A diagram of the flight path, collimation, shielding, sample position and detector locations, is shown in Fig. 2.

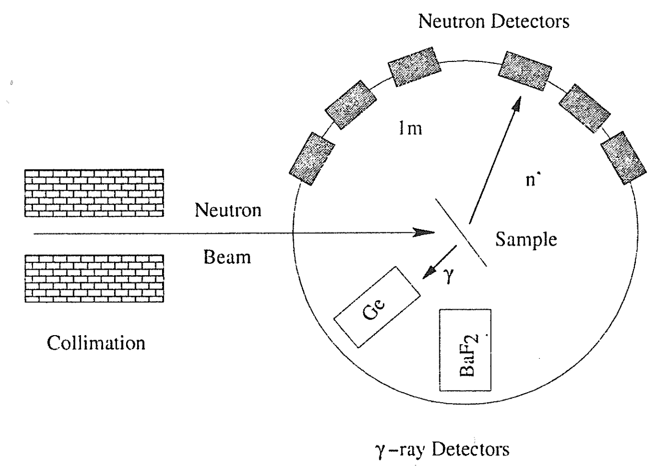


FIG. 2: Experimental Setup.

The silicon target was irradiated at a distance of 21 meters from the neutron production target. The cylindrical sample was 5-cm high and 2-cm in diameter. The experimental approach was as follows : A pulse of neutrons having a wide energy spectrum is produced in the Target-4 spallation neutron source at WNR by the interaction of the 800 MeV proton beam from the LANSCE accelerator with a tungsten target. The neutrons, collimated to a beam of 1 or 2 cm in diameter, impinge on the natural Si sample, where nuclear excitations take place. The excited nuclei decay by the emission of γ-rays and neutrons $n'$. The γ-rays are detected by one high-resolution Ge or one barium-fluoride detector (see Fig. 3). The emitted neutrons $n'$ are detected in an array of six liquid scintillators at about 1 meter from the sample so that the time of flight (TOF) of $n'$ can be measured and its energy $E_{n'}$ deduced, see Fig. 4 measured from the time of neutron production from the time of gamma-ray trigger.

The TOF of the incident neutron gives the energy $E_n$ at which the reaction is initiated. In the case of $^{28}$Si, the neutron $n'$ signal is recorded in coincidence with the first excited level at 1.78 MeV. Then, using a pulse-shape discrimination (PSD) technique on the liquid scintillator signals, it is possible to separate the gamma-ray pulses from the neutron pulses, see Fig. 5. For PSD, two gates (long and short) are used on the time pulse from the liquid scintillators. As the fraction of light appearing in the slow component depends on the nature of the incident particle, the signals integrated with a short gate and a large gate are plotted with the short gate on the $Y$-axis and the long gate on the $X$-axis. The signals induced by the gamma rays and neutrons are then separated. The number of neutron-induced pulses are then divided by the neutron detector efficiency and the beam flux to obtain the total neutron yield.

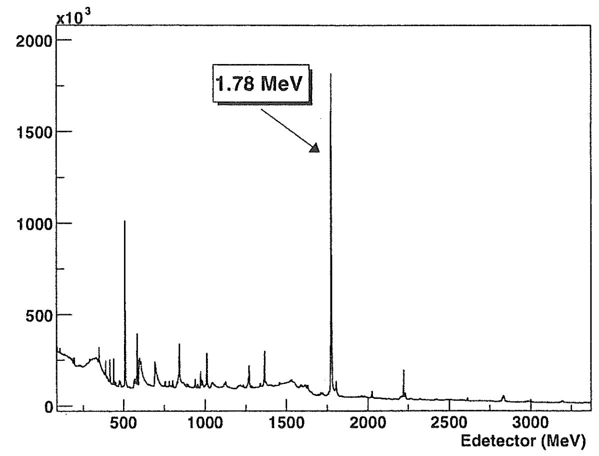


FIG. 3: Gamma-ray spectrum from the Ge detector for the decay of $^{28}$Si. The line at 1.78 MeV arises from decays of the first excited state in $^{28}$Si.

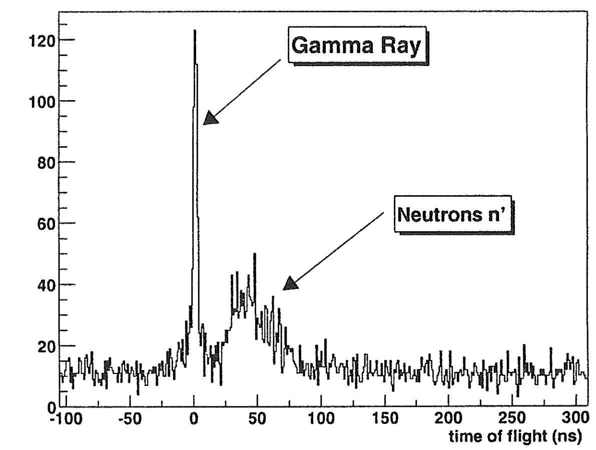


FIG. 4: Time of flight for the neutron $n'$ between the target and a sample neutron detector. The narrow peak for the coincidence gamma rays and a broader neutron time of flight distribution are marked. For $t > 100$ ns, only the background is present.

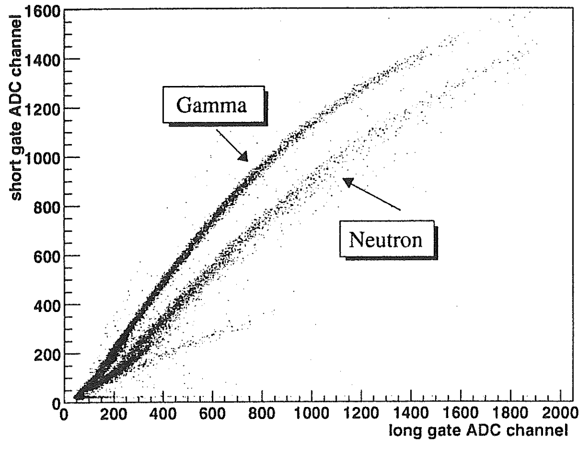


FIG. 5: Pulse shape discrimination on a liquid scintillator EJ301 during the measurements. Two gates on the time pulse are used : a short gate in $Y$-axis and a long gate in $X$-axis.

### *I. B. Data normalizations*

In the experiment, six neutron detectors, containing EJ301 liquid scintillator (2 inches thick, 5 inches in diameter of active scintillator), similar to NE213,[13,14] were used. The neutron efficiency was measured using the fission neutrons from a spontaneous fission source of $^{252}$Cf as a standard.[15]

The second data normalization is a function of the neutron beam intensity. The neutron beam was monitored with a large fission chamber[16] using the fission of $^{235}U$ and $^{238}U$. The TOF between the neutron production target and the fission chamber is used to calculate the incident neutron energy. The deduced spectrum is presented on Fig. 6. This spectrum is then used to normalize the Si data to obtain beam-independent data.

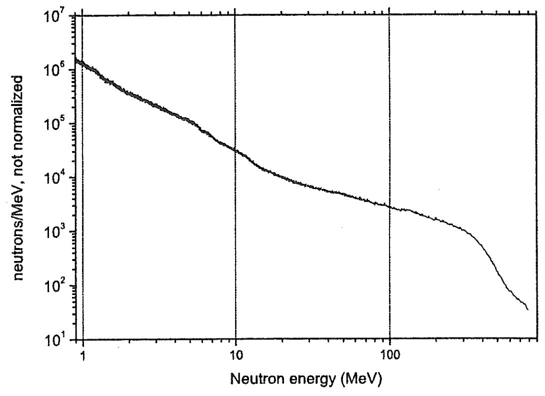


FIG. 6: Neutron flux (not normalized) as a function of the neutron kinetic energy.

### *I. C. Data reduction*

A cut in TOF to remove all events with outgoing neutron kinetic energy less than 1 MeV was applied to reduce the background. In order to sum the data from all neutron detectors, we present the data as a plot of the excitation energy $E_x$ of the residual nucleus $^{28}$Si* as a function of the incident neutron energy $E_n$. $E_x$ is evaluated by subtracting the ground state mass from the invariant mass of the residual of the reaction $^{28}$Si$(n, n')$. The momentum of the detected gamma-ray is not included in the kinematics.

Furthermore, in order to correct for the background at all incident neutron energies, several measurements were done without the sample, with the neutron beam on. This background, suitably normalized, was subtracted from the $^{28}$Si sample measurements. By subtraction of the ground state energy from the total energy, the excitation energy $E_x$ as a function of $E_n$ is available and is presented in Fig 7.

In order to extract data proportional to the cross section from the $E_x$-$E_n$ matrix, one-dimensional energy spectra were generated by summing TOF bins corresponding to a "slice" in neutron energy, and projecting onto the excitation energy axis ($Y$-axis). Then, the excitation energy distribution for a given incident neutron energy is compared with the GNASH and EMPIRE-II calculations.

## III. CALCULATIONS

### *III. A. Statistical model calculations*

Model calculations for neutron reactions on silicon were performed with two different codes, EMPIRE II[17] and GNASH.[18,19]

EMPIRE-II is a statistical model code for nuclear reaction calculations.[17] EMPIRE-II includes various nuclear models, designed for calculations in a broad range of energies and incident particles. The version used here (EMPIRE II.16.2) includes the spherical optical model SCAT2,[20] coupled channels (ECIS),[21] Multistep Direct (ORION + TRISTAN)[22] mechanisms, Monte Carlo preequilibrium emission, and the full featured Hauser-Feshbach model with width fluctuation correction. A comprehensive library of input parameters covers nuclear masses, optical model parameters, ground state deformations, discrete levels and decay schemes, level densities, moments of inertia, and $\gamma$-ray strength functions. EMPIRE II is used here with the default parameters to calculate the inelastic cross section $^{28}$Si$(n, n')^{28}$Si and neutron emission spectra. For incident neutron energy less than 10.3-MeV, the reactions $^{28}$Si$(n, n'\alpha)^{24}$Mg and $^{28}$Si$(n, n'p)^{27}$Al are not allowed and the results from EMPIRE II can be directly compared with the measurements on FIGARO. For incident neutron energies higher than the 10.3-MeV



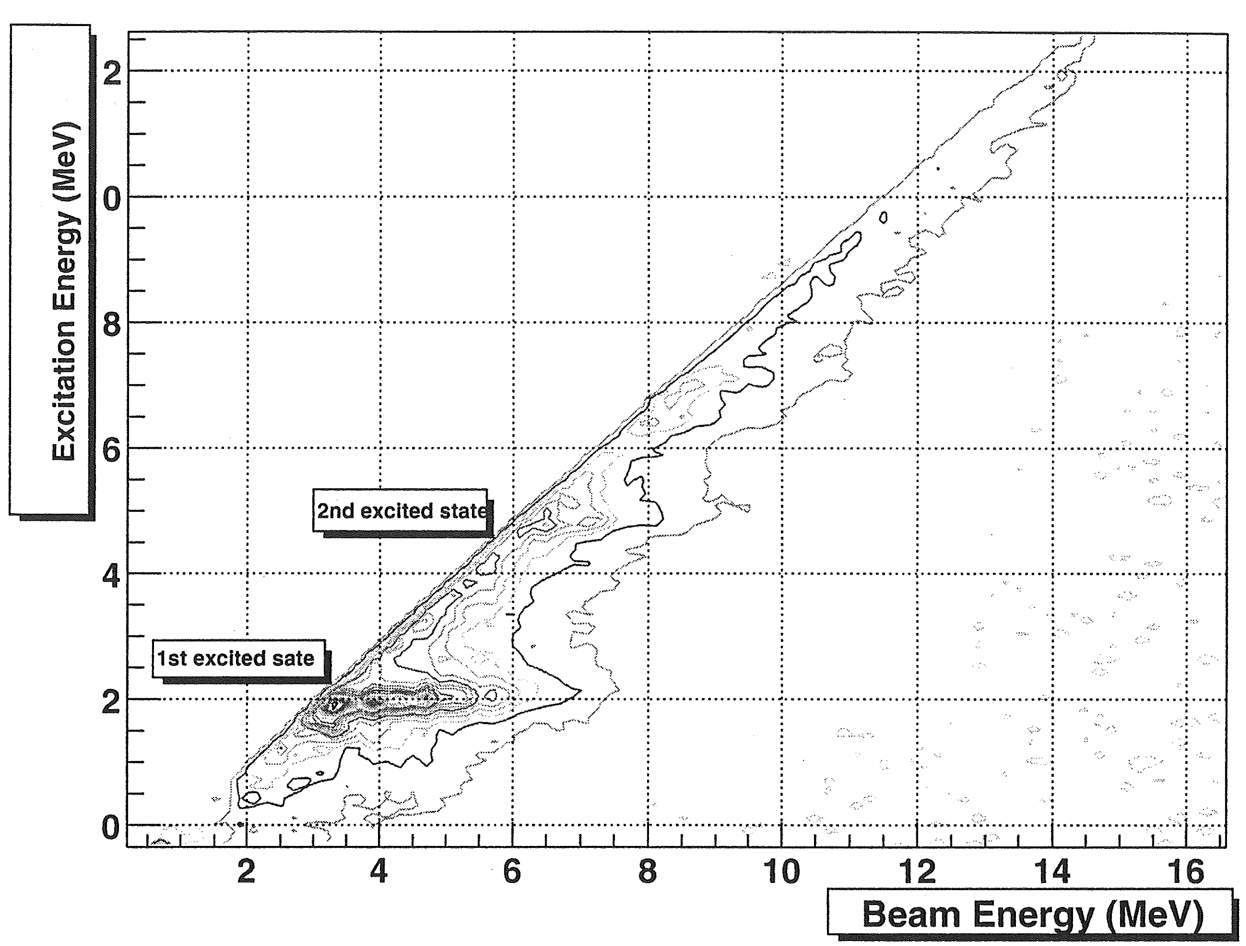


FIG. 7: Excitation energy of the residual nucleus $^{28}$Si in MeV as a function of the incident neutron energy in MeV after normalization. See specially the excited levels at 1.78 MeV and 4.62 MeV with 4.98 MeV.

threshold, the $(n, n'\alpha)$ channel is opened and is in competition with the neutron inelastic scattering on $^{28}$Si. The measured cross sections on FIGARO will then be different from the calculated results, which include all the possible channels $(n, n'x)$. The $(n, n'p)$ channel further complicates the comparison above 12.5 MeV.

The GNASH preequilibrium-statistical model code applies Hauser-Feshbach compound nucleus theory to describe the decay of equilibrated nuclei and the exciton model for the emission of higher-energy preequilibrium ejectiles in the early stage of the reaction.[23] Preequilibrium corrections based upon the exciton model of Kalbach,[24] modified to include nuclear surface effects, are applied to the decay of the first compound nucleus. The Hauser-Feshbach calculation accounts for sequential multiparticle and $\gamma$-ray decay until secondary emission is complete and the residual nucleus is left in its ground state. Up to six types of radiation can be emitted from each compound system so that in one calculation a maximum of 60 reaction paths can be treated. The GNASH calculations were performed by M. Chadwick and P. Talou from the Theoretical Division T-16 of the LANL.[25]

### *III. B. Code-measurement comparisons*

For both codes GNASH and EMPIRE-II, the calculations provide neutron emission intensities with narrow distributions corresponding to excitation of discrete levels. The output of the codes give widths corresponding to the energy steps in the calculations. For the measurements, the width of the neutron distribution in the discrete excited levels region comes from the resolution given by the time of flight between the Si target and the neutron detectors. As the distance for this TOF is constant (approximately 1 m), the resolution is a function of the outgoing neutron energy $E_{n'}$. The resolution is better for slow neutrons and worse for fast neutrons. In terms of the excitation energy of the residual nucleus,for a given incident neutron energy, this corresponds to a better resolution for a high value of the excitation energy.

In order to compare the measurements with the calculations, a convolution is performed between the $\gamma$-peak of the discrete excited levels and a Gaussian function with the following parameters :

- centroid equal to the $\gamma$-peak centroid
- area equal to the $\gamma$-peak area
- width $\sigma_E$ determined by the TOF resolution for the neutron detector to Si target distance. With the hypothesis that the width of the Gaussians is only equal to the time of flight resolution, the width is :

$$\begin{aligned}\sigma_{E_{n'}} &= \Delta E_{n'} \\ &= 2E_{n'}\Delta t/t\end{aligned}$$

With $t = \sqrt{\frac{ml^2}{2E_{n'}}}$, $m$ the neutron mass, $l$ the distance neutron detector-Si target and $\Delta t$ equal to the time resolution, $\sigma_E$ is then equal to :

$$\sigma_{E_{n'}} = 4 \cdot 10^{-2} * E_{n'}^{3/2} \qquad (1)$$

where the energy units are MeV. In the continuum region, the excitation of the residual nucleus is high compared to the discrete levels region and the resolution for the outgoing neutron energy is rather good. In consequence, the widths of the Gaussian functions in this energy region are small enough not to enlarge the results of the GNASH and EMPIRE-II calculations.

Furthermore, as explained in the introduction, most of the decays of the excited states of $^{28}$Si go through its first excited state. Only four decays go directly to the ground state:[26]

- 6.88-MeV ($3^-$) with a branching ratio of 70 %
- 7.38-MeV ($2^+$) with a branching ratio of 36 %
- 7.41-MeV ($2^+$) with a branching ratio of 94 %
- 7.93-MeV ($2^+$) with a branching ratio of 83 %

In consequence, in order to compare the calculations from EMPIRE II and GNASH, the intensities corresponding to the population of these four excited levels and their branching ratios have to be subtracted from the results of the two codes. This was done in the analysis.

## IV. RESULTS AND DISCUSSION

As explained in paragraph II, neutron-emission spectra as a function of the residual excitation energy can be obtained from Fig. 7 for a given incident neutron energy.

For excitation energies higher than 8-MeV, the excited levels are no longer discrete and become a continuum region with observable peaks. In order to obtain data proportional to the inelastic neutron scattering cross section as a function of the $^{28}$Si excitation energy for a given incident neutron kinetic energy, narrow slices are projected on the $Y-$axis in Fig. 7 for incident neutron energies in the range $E_n$ to $E_n + k$. For $E_n$ less than 7 MeV the slice widths $k$ are equal to 200 keV and for higher $E_n$, because of the lower statistics, the slice widths $k$ are equal to 1 MeV. Emission spectra are given in Figs. 8, 9 and 10.

### *IV. A. FIGARO-EMPIRE II-GNASH Comparisons*

Because the 1.78 MeV gamma-ray has an angular distribution not included in the calculations, we need to normalize experiments and calculations. Up to 13 MeV, the FIGARO data are normalized to the mean value given by the integration of EMPIRE II and GNASH data over the excitation energies for a given incident neutron energy. For higher energies, as the EMPIRE II and GNASH data are the sum of $(n,n')$, $(n,n'\alpha)$ and $(n,n'p)$, the FIGARO data are not normalized to EMPIRE II and GNASH, but are presented on the same graph and are arbitrarily normalized to compare the shape of each distribution and not the intensities.

First of all, it is interesting to notice that EMPIRE II and GNASH do not give the same intensities for the discrete level distribution or for the continuum region. The input parameters for GNASH have been chosen to give good agreement with previous experimental data on $^{28}$Si(n,$x\alpha$) and $^{28}$Si(n,$x$p)[27], whereas for EMPIRE II the input parameters are chosen by default.

In the case where only the $(n,n')$ channel is open, *i.e.* for incident neutron energies lower than 10 MeV, the measurements show a good agreement with the calculations. Several peaks are well defined : 1.78 MeV, 4.61 mixed with 4.98 MeV, 6.27 MeV and 6.69 MeV. For excitation energy higher than 8 MeV, the energy spacings between levels are too small to allow a peak separation and the continuum region begins. The opening of the $(n,n'\alpha)$ and $(n,n'p)$ channels (see Fig. 1) will induce a difference between the calculations and the measurements; both calculation codes provide the energy distribution of the first emitted neutron from $^{29}$Si, without a coincidence window on the transition $\gamma$-ray between the first excited state and the ground state following the $\gamma$-ray cascade in $^{28}$Si. In consequence, the codes provide the first-neutron-emission cross section, which differs from the inelastic neutron cross section.

In the region of incident neutron energies above 14 MeV, the FIGARO data present a different shape than the calculations because the first one gives the $^{28}$Si$(n,n'\gamma)^{28}$Si excitation function and the calculations provide all the decays $^{28}$Si$(n,n')$, $^{28}$Si$(n,n'xp)$ and $^{28}$Si$(n,n'x\alpha)$. The presented measured data cannot be normalized to the calculations; only the shapes of the distributions are comparable.



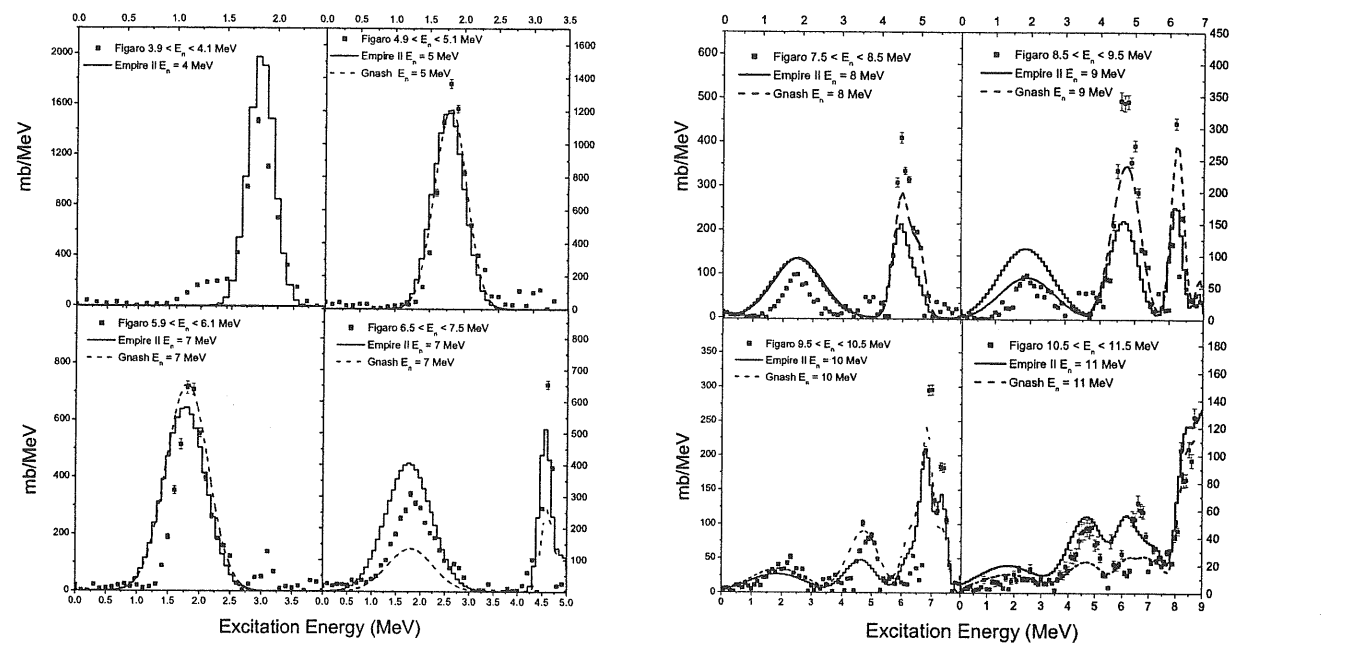


FIG. 8: Angle-integrated neutron inelastic scattering spectra for neutron energies from 4 to 11 MeV, normalized to the mean value of the calculations. The solid line depicts the results of EMPIRE II and GNASH calculations when available, performed at the midpoint of the respective neutron energy bin; a convolution is performed with the resolution of the measurement.

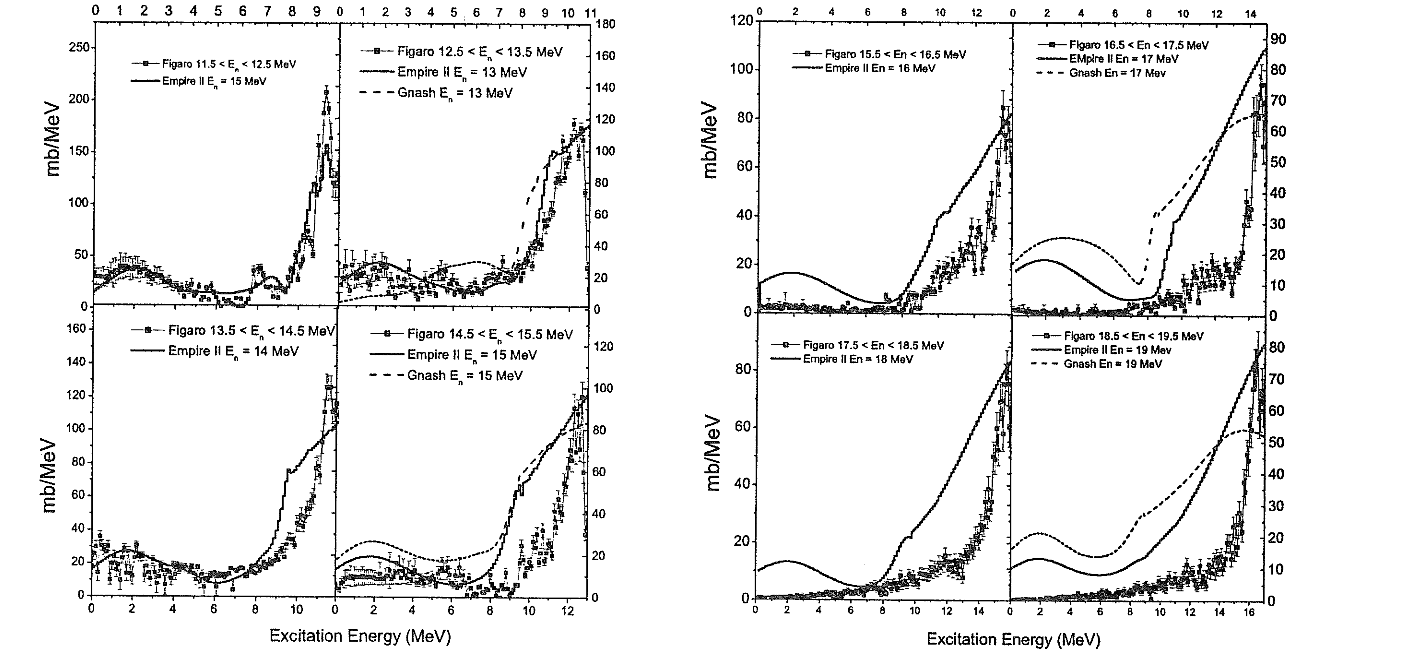


FIG. 9: Angle-integrated neutron inelastic scattering spectra for neutron energies from 12 to 19 MeV, normalized to the mean value of the calculations up to 13 MeV. The solid line depicts the results of EMPIRE II and GNASH calculations when available, performed at the midpoint of the respective neutron energy bin; a convolution is performed with the resolution of the measurement.

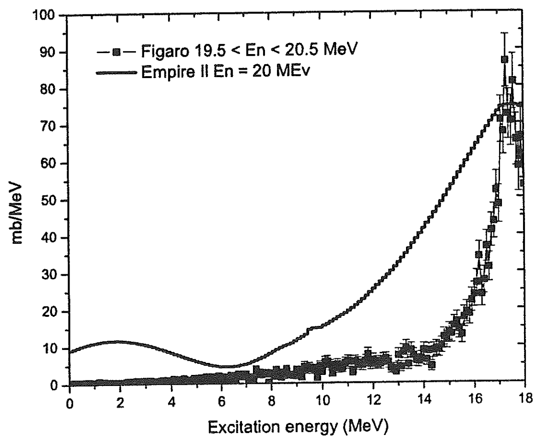


FIG. 10: Angle-integrated neutron inelastic scattering spectra for neutron energies of 19.5-20.5, MeV. The solid line depicts the results of EMPIRE II and GNASH calculations when available, performed at the midpoint of the respective neutron energy bin, and convoluted with the resolution of the measurement.

*IV. B. Comparison with the literature data*

As the FIGARO data are proportional to the inelastic cross section and depend on the gamma-ray detection efficiency, only the simulations with EMPIRE II and GNASH can be compared with the absolute data from the literature.

For 14.1 MeV, the neutron emission spectrum from A. Takahashi[11] can be compared to the results of the EMPIRE II calculations for $E_n = 14$ MeV. This comparison is presented in Fig. 11.

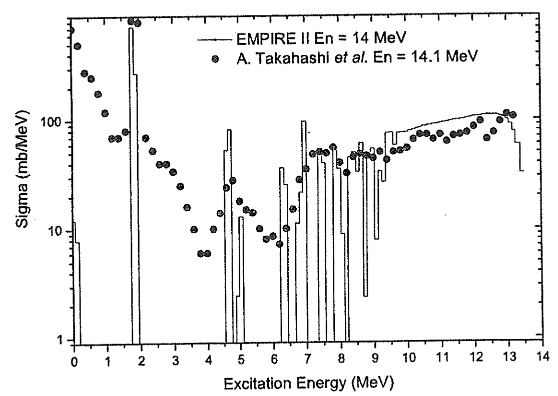


FIG. 11: Comparison between EMPIRE II for $E_n = 14$ MeV and data from Ref. 11 for $E_n = 14.1$ MeV.

The calculation from EMPIRE II and the data from Ref. 11 are in rather good agreement. The neutron emission spectrum for excitation energies less than 3 MeV has a large component from the tail of the elastic scattering peak.

## V. CONCLUSION AND PERSPECTIVES

These measurements on FIGARO provide new information on the excitation functions of the neutron emission spectra for $^{28}\mathrm{Si}(n,n')^{28}\mathrm{Si}$ in coincidence with the first excited state $2^+$ of the $^{28}$Si for incident neutron energies from 4 to 20 MeV. Comparisons with the reaction model codes GNASH and EMPIRE II show a good agreement for incident energies where only the $(n,n')$ channel is opened. The two codes GNASH and EMPIRE II present some discrepancies for the intensities of neutron distributions in the discrete region and of the continuum region which could be due to the default parameters used for EMPIRE II. The planned upgrade of FIGARO with another Ge detector and 49 neutron detectors will provide better statistics on the neutron emission spectrum and will allow the use of natural elements with several isotopes such as molybdenum.


### Acknowledgments

We wish to thank M. Chadwick and P. Talou from the theoretical group in T-16, LANL, for their collaboration and support for the GNASH calculations.


### REFERENCES


1. P. W. LISOWSKI, C. D. BOWMAN, G. J. RUSSELL and S. A. WENDER, "The Los Alamos National Laboratory Spallation Neutron Sources", Nucl. Sci. Eng. **106**, 208 (1990)

2. J. F. ZIEGLER and W. A. LANFORD, "Effect of Cosmic Rays on computer memories", Science **206**, 776 (1979)

3. N. B. SULLIVAN, J. J. EGAN, G. H. R. KEGEL and P. HARIHAR, "Neutron Inelastic Scattering on Silicon-28 to 4.15 MeV", Nucl. Sci. Eng. **70**, 294 (1979)

4. H. H. KNITTER and M. COPPOLA, "Neutron Scattering from Natural Silicon", Z. Phys. **207**, 56 (1967)

5. D. M. DRAKE, J. C. HOPKINS, C. S. YOUNG, H. CONDE and A. SATTLER, "Fast neutron elastic and inelastic scattering from silicon", Nucl. Phys. **128**, 209 (1965)

6. S. C. MATHUR, W. E. TUCKER, R. W. BENJAMIN and I. L. MORGAN, "Angular distribution of gamma rays produced by neutron bombardment of Al, Mg and Si", Nucl. Phys. **73**, 561 (1965)

7. J. MARTIN, D. T. STEWART and W. M. CURRIE, "Scattering of 6 MeV neutrons from light nuclei", Nucl. Phys **A 113**, 564 (1968)

8. S. KLICZEWSKI and Z. LEWANDOWSKI," Elastic and inelastic scattering of 14.1 MeV neutrons on $^{28}$Si nuclei in a wide angular range and the spin-orbit interaction," Nucl. Phys. **A 304**, 269 (1978)

9. G. A. PETITT, S. G. BUCCINO, G. E. HOLLANDSWORTH and P. R. BEVINGTON, "Elastic and inelastic neutron scattering by silicon and sulphur", Nucl. Phys. **79**, 231 (1966)

10. D. SEELIGER, D. SCHMIDT and T. STREIL, "Nuclear structure and direct reaction mechanism in neutron scattering on $^{28}$Si in the range 6.8 to 14.8 MeV", Nucl. Phys. **A 460**, 265 (1986)

11. A. TAKAHASHI, E. ICHIMURA, Y. SASAKI and H. SUGIMOTO, "Double and Single Differential Neutron Emission Cross Section at 14.1 MeV", *V*olume-1, OKTAVIAN Report A-87-03, Osaka University, Nov. 1987

12. R. C. HAIGHT, M. DEVLIN, J. M. O'DONNELL, T. ETHVIGNOT and T. GRANIER, "FIGARO-A fast Neutron-Induced Gamma-Ray Observer", LANL Internal Report LALP-02-174, 2002

13. D. T. INGERSOLL and B. W. WEHRING, "Gamma-ray Pulse-Height response of an NE-213 scintillation detector", Nucl. Inst. and Meth. **147**, 551 (1977)

14. K. H. MAIER and J. NITSCHKE, "Die Lichtausbeute eines NE 213-szintillators für Protonen", Nucl. Inst. and Meth. **59**, 227 (1968)

15. Nuclear Data Standards for Nuclear Measurements, NEA Nuclear Data Committee, NEANDC/INDC, 1991

16. S. A. WENDER, S. BALESTRINI, A. BROWN, R. C. HAIGHT, C. M. LAYMON, T. M. LEE, P. W. LISOWSKI, W. McCORKLE, R. O. NELSON and W. PARKER, "A fission ionization detector for neutron flux measurements at a spallation source", Nucl. Instrum. Meth. in Phys. Res. **A 336**, 226 (1993)

17. M. HERMAN, R. CAPOTE-NOY, P. OBLOŽINSKÝ, A. TRKOV and V. ZERKIN, "Recent Development and Validation of the Nuclear Reaction Code EMPIRE", International Conference on Nuclear Data for Science and Technologie, Tsukuba, Oct, 2001

18. P. G. YOUNG and E. D. ARTHUR, "A Preequilibrium, Statistical Nuclear-Model Code for Calculation of Cross Sections and Emission Spectra", LANL Internal Report LA-6947-C.3, 1977

19. E. D. ARTHUR, "The GNASH Preequilibrium-Statistical Model Code", LANL Internal Report LA-UR-88-382, 1988

20. O. BERSILLON, "*SCAT2* : Un programme de modèle optique sphérique", Report CEA-N-2227, NEANDC(FR), INDC(E) 49/L, Oct 1981

21. J. Raynal,"Notes on *ECIS*", Report CEA-N-2772, 1994

22. T. TAMURA, T. UDAGAWA and H. LENSKE, "Multistep direct reaction analysis of continuum spectra in reactions induced by light ions", Phys. Rev. **C 26**, 379 (1982)

23. P. G. YOUNG, E. D. ARTHUR and M. B. CHADWICK, "Comprehensive nuclear model calculation: Introduction to the theory and use of GNASH code", LANL Internal Report LA-12343-MS, 1992

24. C. KALBACH, "The Griffin Model, Complex Particles and Direct Nuclear Reactions", Z. für Physik **A 283**, 401 (1977)

25. M. CHADWICK and P. TALOU, Private communication 2002

26. P. M. ENDT, "Supplement to energy levels of $A = 21 - 44$ Nuclei (VII)", Nucl. Phys. **A 633**, 1 (1998)

27. F. B. BATEMAN, R. C. HAIGHT, M. B. CHADWICK, S. M. STERBENZ, S. M. GRIMES and H. VONACH, "Light charged-particle production from neutron bombardment of silicon up to 60 MeV: Role of level densities and isospin", Phys. Rev. **C 60**, 064609